Inorg. Chem. **2005**, *44*, 2003–2011

Enhanced Photoluminescence from Group 14 Metalloles in Aggregated and Solid Solutions

Henry J. Tracy,[†] Jerome L. Mullin,*[,‡] Wim T. Klooster,[§] James A. Martin,[‡] Judith Haug,[‡] Scott Wallace,[†] Isaac Rudloe,[†] and Kimberly Watts[†]

Department of Chemistry, University of Southern Maine, Portland, Maine 04104, Department of Chemistry, University of New England, Biddeford, Maine 04005, and Bragg Institute, Australian Nuclear Science and Technology Organisation, Menai, NSW, Australia

Received July 20, 2004

The unusual photoluminescence characteristics of a series of six group 14 metalloles (1,1-dimethyl-2,3,4,5-tetraphenylmetalloles and 1,1-diphenyl-2,3,4,5-tetraphenylmetalloles) containing silicon, germanium, or tin have been investigated. Although the compounds are weakly luminescent in dilute fluid solution at room temperature, they undergo a substantial enhancement of photoluminescence when forced to aggregate, as in mixed solvent systems. The compounds also exhibit considerable emission when incorporated into rigid room-temperature glasses of sucrose octaacetate. Absorption and emission characteristics of the compounds, including luminescence quantum yields, in fluid solution, solution-phase aggregates, and room-temperature glasses are reported. Quantum yields increase by as much as 2 orders of magnitude in the aggregates and glasses, compared to fluid solution. Experimental evidence supports the conclusion that the aggregation-induced enhancement of luminescence results from restricted intramolecular rotations in the packed metalloles. The unusual aggregation-induced enhancement of these compounds makes them potentially useful for the fabrication of a variety of electrooptical devices and sensors. In addition, the X-ray crystal structure of hexaphenylgermole is reported.

Introduction

First synthesized by Braye[1] and Leavitt[2,3] in the late 1950s, group 14 metalloles, silicon-, germanium-, or tin-containing metallacyclopentadienes,[4,5] have received renewed attention recently because of their unusual electronic structure and resulting photophysical characteristics[6−9] and their use as building blocks for the construction of π-conjugated polymers.[6,8] Siloles, in particular, are of significant current interest because they exhibit high electron affinity and fast electron mobility,[10] leading to their use as electron-transporting and light-emitting materials for the fabrication of organic electroluminescent devices.[10−13] Among the most efficient single emitter-based organic light-emitting diodes (OLEDs) are some recently reported silole-based devices.[12,13] The unusual optical behavior of the siloles is a consequence of their low-lying LUMO levels, which result from $\sigma^*-\pi^*$ conjugation between the σ^* orbital of the two exocyclic σ bonds on the ring Si and the π^* orbital of the butadiene moiety,[7,11,14] in sharp contrast to the electronic structure of cyclopentadiene itself.[4] Historically, germoles and stannoles have received

* To whom correspondence should be addressed. Department of Chemistry, University of New England, Biddeford, ME 04005; e-mail, jmullin@une.edu.
[†] University of Southern Maine.
[‡] University of New England.
[§] Australian Nuclear Science and Technology Organisation.

(1) Braye, E. H.; Hubel, W.; Caplier, I. *J. Am. Chem. Soc.* **1961**, *83*, 4406−4413.
(2) Leavitt, F. C.; Manuel, T. A.; Johnson, F. *J. Am. Chem. Soc.* **1959**, *81*, 3163−3164.
(3) Leavitt, F. C.; Manuel, T. A.; Johnson, F.; Matternas, U.; Lehman, D. S. *J. Am. Chem. Soc.* **1960**, *82*, 5099−5102.
(4) Dubac, J.; Laporterie, A.; Manuel, G. *Chem. Rev.* **1990**, *90*, 215−264.
(5) Colomer, E.; Corriu, R. J. P.; Lheureux, M. *Chem. Rev.* **1990**, *90*, 265−282.
(6) Yamaguchi, S.; Tamao, K. *J. Chem. Soc., Dalton Trans.* **1998**, 3693−3702.
(7) Yamaguchi, S.; Itami, Y.; Tamao, K. *Organometallics* **1998**, *17*, 4910−4916.
(8) Sohn, H.; Sailor, M. J.; Magde, D.; Trogler, W. C. *J. Am. Chem. Soc.* **2003**, *125*, 3821−3830.
(9) Yamaguchi, S.; Endo, T.; Uchida, M.; Izumizawa, T.; Furukawa, K.; Tamao, K. *Chem.—Eur. J.* **2000**, *6*, 1683−1692.
(10) Chen, J.; Law, C. C. W.; Lam, J. W. Y.; Dong, Y.; Lo, S. M. F.; Williams, I. D.; Zhu, D.; Tang, B. Z. *Chem. Mater.* **2003**, *15*, 1535−1546.
(11) Yamaguchi, S.; Jin, R.-Z.; Tamao, K. *J. Organomet. Chem.* **1998**, *559*, 73−80.
(12) Chen, H. Y.; Lam, W. Y.; Luo, J. D.; Ho, Y. L.; Tang, B. Z.; Zhu, D. B.; Wong, M.; Kwok, H. S. *Appl. Phys. Lett.* **2002**, *81*, 574−576.
(13) Murata, H.; Kafafi, Z. H.; Uchida, M. *Appl. Phys. Lett.* **2002**, *81*, 189−191.

10.1021/ic049034o CCC: $30.25
Published on Web 02/22/2005

limited attention,[15] but more recently, they, too, have become subjects of greater interest, as they display the same unusual optical properties as do the siloles.[4,5,8,16]

There has been great interest in synthesizing π-conjugated polymers containing silole monomers analogous to polythiophene and polypyrrole. Theoretical studies on 2,5-polysiloles suggest that they would possess properties such as low-band gaps, nonlinear optical properties, and thermochromism.[6] Both polymetalloles and metallole−silane copolymers recently have been reported.[6,8,16−20] Many of these materials, particularly the linear polymers, are highly luminescent, have high-electron or -hole mobility, and show high nonlinear optical susceptibility, making them excellent candidates for use as light-emitting diodes (LEDs) or chemical sensors.

Lumophores used for fabrication of electroluminescent devices should have high photoluminescence (PL) quantum yields and be thermally stable, nontoxic, robust, economically synthesized, and easily fabricated into solid-state devices. The ability to tune the emission wavelength of the lumophore would be an added benefit. One of the greatest problems encountered in the fabrication of such devices is the aggregation-induced quenching of emission characteristic of most lumophores, which results in decreasing emission intensity as the lumophores are increasingly forced to aggregate (e.g., in poor solvents or solid-state devices). Even in the fabrication of thin films, some aggregation usually is unavoidable.[15] An unusual aspect of metallole behavior recently reported is the significant aggregation-induced *enhancement* (AIE) of photoluminescence from a variety of silole derivatives.[10,12,13,15,19−21] The AIE effect also has been reported to occur in 1,1-diethynyl-2,3,4,5-tetraphenylgermole.[16] This atypical behavior could be of considerable value in the development of devices such as LEDs and sensors. As noted above, siloles are particularly attractive for device fabrication because of their high electron acceptability and fast electron mobility; the ability to greatly increase their PL efficiency via aggregation could make them even more useful in a variety of optoelectronic applications. The lack of aggregation-induced self-quenching problems greatly facilitates the preparation of optoelectronic devices. For example, polymers incorporating metalloles have been prepared in attempts to construct simple, efficient photoluminescent and electroluminescent devices.[16,19,20] While some linear silole-based polymers have been observed to exhibit the AIE effect,[19,20] hyperbranched poly(phenylenesilolene)s and poly(phenylenegermole)s do not show enhanced emission when aggregated.[16,20] The AIE phenomenon has been attributed to restricted intramolecular rotations resulting from the packing of the propeller-shaped metalloles in the aggregates.[10,15,16,19,20] In addition to the potential of exploiting the AIE effect, it should be possible to tune the emission wavelengths of suitable siloles (or other metalloles) by changing the identity of the 2,5-substituents.[22]

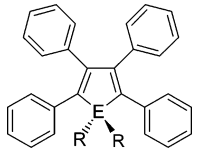

Figure 1. Generalized structure of the group 14 metalloles. E represents Si, Ge, or Sn; R is methyl or phenyl.

Previously, we reported weak luminescence from a series of six siloles, germoles, and stannoles (Figure 1), in dilute fluid solutions at room temperature.[23] Luminescence quantum yields for these compounds are reported below. The work described herein also explores the AIE effect in this set of metalloles. For simplicity, the six compounds in the series are designated by specifying the group 14 element and the identity of the 1,1-substituents (the 1,1-substituents, either methyl or phenyl groups, occur in matched pairs in this series of compounds). Thus, the compounds are identified as SiMe, GeMe, SnMe, SiPh, GePh, and SnPh. We previously reported the synthesis, ^{1}H and ^{13}C nuclear magnetic resonance spectra, and electrochemical behavior of these compounds, as well as the crystal structure of SnPh.[23] Although the siloles demonstrate the most dramatic AIE of PL, the effect also is pronounced in the germoles and stannoles. Even SnMe, which is essentially nonluminescent in fluid solution at room temperature, becomes quite emissive when aggregated.

In an effort to characterize more thoroughly the luminescence properties of these metalloles and elucidate further the reasons for the unusual AIE phenomenon, the optical characteristics of the compounds have been studied in a variety of solvents and in rigid room-temperature glasses, solid pellets, and low-temperature (frozen) solutions. The crystal structure of GePh is reported here; this crystal structure, that of SnPh,[23] and a redetermination of the crystal structure of SiPh provide insight into the mechanism by which aggregation may influence the emission characteristics of the compounds.

Experimental Section

A. Reagents. The group 14 metalloles were prepared and purified as described previously.[23] Acetonitrile, tetrahydrofuran, dioxane, benzene, and dichloromethane were spectrophotometric- or HPLC-grade, obtained from Aldrich, Acros, or EM Scientific. Absolute ethanol was obtained from Pharmco. Quinine sulfate, used as the quantum yield standard, was supplied by Fisher Scientific. Sucrose

(14) Tang, B. Z.; Zhan, X.; Yu, G.; Lee, P. P. S.; Liu, Y.; Zhu, D. *J. Mater. Chem.* **2001**, *11*, 2974−2978.
(15) Luo, J.; Xie, Z.; Lam, J. W. Y.; Cheng, L.; Chen, H.; Qui, C.; Kwok, H. S.; Zhan, X.; Liu, Y.; Zhu, D.; Tang, B. Z. *Chem. Commun.* **2001**, 1740−1741.
(16) Law, C. C. W.; Chen, J.; Lam, J. W. Y.; Peng, H.; Tang, B. Z. *J. Inorg. Organomet. Polym.* **2004**, *14*, 39−51.
(17) Sohn, H.; Huddleston, R. R.; Powell, D. R.; West, R.; Oka, K.; Yonghua, X. *J. Am. Chem. Soc.* **1999**, *121*, 2935−2926.
(18) Sanji, T.; Sakai, T.; Kabuto, C.; Sakurai, H. *J. Am. Chem. Soc.* **1998**, *120*, 4552−4553.
(19) Chen, J.; Xie, Z.; Lam, J. W. Y.; Law, C. C. W.; Tang, B. Z. *Macromolecules* **2003**, *36*, 1108−1117.
(20) Chen, J.; Peng, H.; Law, C. C. W.; Dong, Y.; Lam, J. W. Y.; Williams, I. D.; Tang, B. Z. *Macromolecules* **2003**, *36*, 4319−4327.
(21) Lee, M. H.; Kim, D.; Dong, Y.; Tang, B. Z. *J. Korean Phys. Soc.* **2004**, *45*, 329−332.
(22) Tamao, K.; Uchida, M.; Izumizawa, T.; Furukawa, K.; Yamaguchi, S. *J. Am. Chem. Soc.* **1996**, *118*, 11974−11975.
(23) Ferman, J.; Kakareka, J. P.; Klooster, W. T.; Mullin, J. L.; Quattrucci, J.; Ricci, J. S.; Tracy, H. J.; Vining, W. J.; Wallace, S. *Inorg. Chem.* **1999**, *38*, 2464−2472.

octaacetate (SOA) from Aldrich was purified by the following procedure:[24] a chloroform solution of SOA (approximately 100 g/200 mL) was passed through a silica gel column (6 cm × 6 cm) and eluted with more chloroform to remove slightly colored impurities. Solvent was removed by rotary evaporation, and the crude product was recrystallized 4 times from absolute ethanol and dried in a desiccator overnight at reduced pressure. The purified SOA (mp = 85−88 °C) was stored away from moisture.

B. Absorption, Excitation, and Emission Characteristics. 1. Instrumentation. Absorbance spectra were obtained using a Perkin-Elmer λ-20 double beam spectrophotometer. Luminescence spectra in fluid solution were collected using 1 cm quartz cuvettes in a Thermo-Spectronic AB-2 spectrofluorometer. Luminescence spectra of the SOA glasses were obtained in 1 cm poly(methyl methacrylate) (PMMA) cuvettes. Other solid-state luminescence spectra were obtained using a variable-angle front surface accessory in the spectrofluorometer. Excitation spectra were ratioed to the instrument's reference channel; all emission spectra reported are corrected spectra.

B.2. Absorption and Emission Characteristics in Room-Temperature Fluid Solutions. Absorption spectra in fluid solutions were collected for a series of dilutions of the compounds in the chosen solvents. Molar absorptivities were obtained by determining the slopes of the resulting Beer's law plots. Approximate quantum yields of luminescence were determined from absorption and emission spectra of the compounds (excited at their absorption maxima) in optically dilute solutions (metallole concentrations approximately 0.01 mM). These relative quantum yields, referenced to quinine sulfate in 0.05 M H_2SO_4 (photoluminescence quantum yield $\Phi_F = 0.55$),[25,26] were determined according to the approach described in the classic work by Demas and Crosby,[25] with careful attention to the cautions noted therein.

B.3. Estimated-Excited State Lifetimes. Preliminary experiments using a PTI LaserStrobe lifetime system indicated that the excited-state lifetimes of the metalloles were less than 200 ps.[27] The luminescence lifetime of GeMe was determined to be 79 ps, using a Spex Fluorolog-τ.[28] These observations are consistent with the 150 ps lifetime recently reported for SiPh by Lee et al.[21] Estimated lifetimes were calculated according to the method described by Strickler and Berg.[29] Their derivation results in the following equation for the reciprocal of the excited-state lifetime (τ_0):

$$\frac{1}{\tau_0} = 2.880 \times 10^{-9} n^2 \langle \tilde{\nu}_f^{-3} \rangle_{A\nu}^{-1} \frac{g_l}{g_u} \int \epsilon \, d \ln \tilde{\nu} \qquad (1)$$

where n is the refractive index of the solution (in applying the equation to dilute solutions, the refractive index of the solvent was used); g_l and g_u are the multiplicities of the lower (ground) and upper (emitting) states, respectively (each of which is equal to 1); the integral is taken over the whole of the electronic absorption band (ϵ is molar absorptivity in L mol^{-1} cm^{-1}; frequency is expressed in cm^{-1}); and the term $\langle \tilde{\nu}_f^{-3} \rangle_{A\nu}^{-1}$ is determined from the emission spectrum according to the following:

$$\langle \tilde{\nu}_f^{-3} \rangle_{A\nu}^{-1} = \frac{\int I(\nu) \, d\nu}{\int \nu^{-3} I(\nu) \, d\nu} \qquad (2)$$

where $I(\nu)$ is the intensity in the emission spectrum. Equation 1 is applicable to molecular species that have strong absorption bands. Because of overlap of absorption bands, the integrated absorbance over the symmetrical band was taken as 2 times the integrated absorbance from the band maximum to the upper wavelength limit of the band.

B.4. Fluid-Phase Aggregates. Fluid-phase aggregates were prepared in mixed solvent systems. While the metalloles are reasonably soluble in acetonitrile, benzene, dioxane, ethanol (except for SiPh, GePh, and SnPh), tetrahydrofuran, and dichloromethane, they are not soluble in water. In mixed solvent systems containing water and one of the water-miscible solvents listed above, the metalloles aggregate. Mixtures were prepared to contain 0, 40, 50, 60, 65, 70, 75, 80, 85, and 90% (v/v) water, with each mixture in a given set containing the same concentration of metallole (typically 0.01 mM). Mixtures with greater than about 60% water effectively scattered laser light, in direct proportion to the amount of water in the system, indicating the formation of uniformly dispersed colloidal-sized aggregates. Although the most extensive studies were carried out using either dioxane or THF as the organic solvent, similar behavior also was observed in water/ethanol and water/acetonitrile systems. The mixtures were stable and remained uniformly dispersed for several hours after preparation.

B.5. Preparation of Room-Temperature Glasses. Dispersions of the metalloles in room-temperature glasses of sucrose octaacetate (SOA) were prepared by melting approximately 5 g of purified SOA powder over gentle heat in a glass beaker, adding a measured amount of metallole solution (typically 50 μL of a 1 mM stock solution in either THF or dioxane), and stirring gently to disperse the metallole. The melt was transferred to a PMMA fluorescence cell, where it quickly hardened into a transparent, glassy solid. The concentrations of the metalloles in the glasses typically were ~0.01 mM. Absorption, excitation, and emission spectra of the glasses were obtained in the same manner as for fluid solutions.

B.6. Frozen Solution Spectra. Frozen solution spectra were obtained by slowly freezing dilute (0.01 mM) dioxane solutions of the metalloles in a freezer to approximately −20 °C or quickly freezing them in liquid nitrogen, directly in PMMA cuvettes. Excitation and emission spectra of the frozen solutions were obtained by placing the cuvettes in the variable-angle front surface accessory in the spectrofluorometer. For comparison, the same solutions also were observed at room temperature in the front surface accessory. Because of the opacity of the frozen solutions, absorption spectra and quantum yields were not obtained.

B.7. Room-Temperature Solid Pellets. Pellets of the metalloles (excluding SnMe) were prepared using nut-and-bolt dies. Excitation and emission spectra were measured using the variable-angle front surface accessory.

C.1. X-ray Crystal Structure of GePh. Yellow crystals of GePh were obtained by recrystallization from 2-propanol. The X-ray data were collected at room temperature using an Enraf-Nonius CAD4 diffractometer with monochromated Cu Kα radiation (λ = 1.5418 Å). The space group was determined to be $P\bar{1}$. The cell parameters (a = 10.279(1) Å, b = 16.529(2) Å, c = 9.641(1) Å; α = 100.23(1)°, β = 108.26(1)°, γ = 77.05(1)°) were obtained by a least-squares fit of $\sin^2\theta$ values for 25 reflections in the range 13° < θ < 17°. Integrated intensities were measured by θ−2θ scans with θ-scan width (1.00 + 0.35 tan θ)°, using varying scan speeds determined by a prescan. Three standard reflections, (−3 0 1), (0 −3 −1), and (1 1 1), were monitored every 60 min. There was no

(24) Kumar, S.; Jones, G. Personal communication.
(25) Demas, J. N.; Crosby, G. A. *J. Phys. Chem.* **1971**, *75*, 991−1024.
(26) Eaton, D. F. *Pure Appl. Chem.* **1988**, *60*, 1107−1114.
(27) Kumar, S.; Jones, G.; Mullin, J. L.; Tracy, H. J. Unpublished results, 2000.
(28) Tracy, H. J.; Mullin, J. L.; Chandler, L. Unpublished result, 2003.
(29) Strickler, S. J.; Berg, R. A. *J. Chem. Phys.* **1962**, *37*, 814−822.

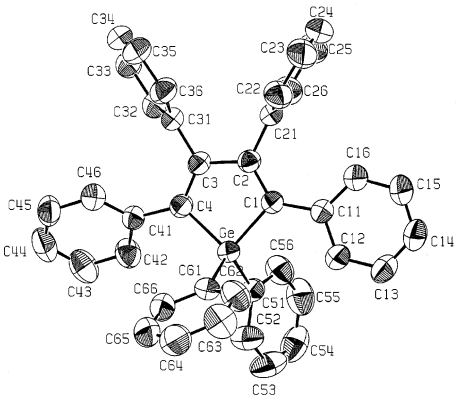

Figure 2. ORTEP diagram of GePh. Thermal ellipsoids are at the 50% probability level. Hydrogens are omitted for clarity.

loss of intensity during the data collection. A hemisphere of data ($\sin\theta/\lambda < 0.60$; $0 \le h \le 12$, $-19 \le k \le 20$, $-12 \le l \le 11$) was collected, yielding a total of 6089 measured reflections, excluding standard reflections. Lorentz, polarization, and absorption corrections were applied. The absorption coefficient, $\mu = 13.90$ cm^{-1}, gave transmission factors in the range 0.941−1.000.[30] Averaging symmetry related reflections gave $R_{int} = 0.032$ and resulted in 6089 independent reflections, 5283 having $F_o^2 > 1.5\sigma(F_o^2)$.

As starting structure, the Sn analogue[23] was used, including hydrogen atoms. Atomic positional, anisotropic displacement parameters for non-hydrogen atoms and isotropic displacement parameters for hydrogen atoms were varied, together with the scale factor, in a full-matrix, least-squares refinement[31] and converged with $\Delta/\sigma < 0.01$. The extinction correction was included but failed to assume a significant value.[32] The quantity $\sum w||F_o^2| - |F_c^2||^2$ was minimized with weights $w = 1/[\sigma^2(F_o^2)]$ and $\sigma^2(F_o^2) = \sigma_{cs}^2 + (0.02F_o^2)^2$, where σ_{cs}^2 is the variance due to counting statistics. Atomic scattering factors were those as calculated by Cromer and Waber.[33] Anomalous dispersion corrections were included.[34] Residual maxima in the final difference Fourier map were 0.5 e Å^{-3} near the Ge atom. The refinement converged with fit indices $R(F_o^2) = 0.059$, $R_w(F_o^2) = 0.090$, and $S = 1.17$.

Results

A. Crystal Structure of GePh. The crystal structure of GePh is consistent with the structures reported previously for SnPh[23] and GeMe.[35] We also determined the crystal structure of SiPh and found it to be consistent with that reported by Chen et al.[10] Crystallographic data for our determination of SiPh are available in the Supporting Information. Figure 2 shows the ORTEP diagram for GePh. Crystallographic data for GePh appear in Table 1. Table 2 summarizes important bond lengths, bond angles, and torsion angles in GePh and, for comparison, SiPh and SnPh. Note, especially, the torsion angles that indicate the relative positions of the four phenyl substituents on the core metallacyclopentadiene ring. All three compounds have remarkably similar conformations in the solid phase. It is perhaps not surprising that the phenyl groups at C2 and C3 (refer to ORTEP diagram for numbering scheme) are positioned at averages of 96.8° (±1) and 63.4° (±2) to the core ring, respectively, because adjacent phenyl substituents could not be coplanar with each other for steric reasons. It is somewhat surprising that the phenyl substituents at C4 are positioned at 46.1° (±0.7) to the core ring. What is even more unexpected, however, is the observation that the phenyl groups at C1 are coplanar with the core ring. Given this observation, it is likely that modification of the substituents at the C4 and especially the C1 positions could have significant effects on the emission wavelengths of the metalloles,[22] since these positions will, due to their geometry,

Table 1. Crystallographic Data for GePh

	GePh
formula	$GeC_{40}H_{40}$
formula mass, au	583.28
space group	$P\bar{1}$
Z	2
a, Å	10.279(1)
b, Å	16.529(2)
c, Å	9.641(1)
α, deg	100.23(1)
β, deg	108.26(1)
γ, deg	77.05(1)
V, Å^3	1505.7(5)
T, °C	25
λ, Å	1.5418
d (calcd), g/cm^3	1.286
Cu Kα (Mo Kα for SnPh)	20 mA, 45 kV
μ, cm^{-1}	13.90
$R(F_o)^a$	0.059
$R_w(F_o)^b$	0.090

[a] $R(F_o^2) = \sum||F_o^2| - |F_c^2||/\sum|F_o^2|$. [b] $R_w(F_o^2) = (\sum w(|F_o^2| - |F_c^2|)^2/\sum w|F_o^2|^2)^{1/2}$.

Table 2. Selected Bond Lengths, Bond Angles, and Torsion Angles for SiPh, GePh, and SnPh[a]

no.		SiPh	GePh	SnPh[b]
	Bond Lengths, Å			
1	E−C1	1.883(1)	1.952(2)	2.134(4)
2	E−C4	1.872(1)	1.947(3)	2.118(5)
3	C1−C2	1.369(2)	1.360(3)	1.355(7)
4	C2−C3	1.507(2)	1.507(3)	1.511(6)
5	E−C51	1.880(1)	1.943(2)	2.127(4)
6	E−C61	1.885(1)	1.958(3)	2.123(5)
	Bond Angles, deg			
1	C1−E−C4	92.96(5)	90.55(9)	84.6(2)
2	E−C1−C2	106.56(8)	106.6(1)	107.2(3)
3	E−C4−C3	107.5(1)	107.2(2)	107.9(3)
4	C1−C2−C3	116.75(9)	117.9(2)	120.0(4)
5	C2−C3−C4	116.1(1)	117.6(2)	119.9(4)
6	C51−E−C61	111.93(6)	112.3(1)	112.3(2)
	Torsion Angles, deg			
1	E−C1−C11−C12	−0.9(2)	−0.7(3)	−1.2(6)
2	E−C4−C41−C42	−46.3(2)	−45.3(3)	−46.6(7)
3	C1−C2−C21−C26	95.8(2)	97.0(3)	97.7(7)
4	C2−C3−C31−C36	−62.4(2)	−62.3(3)	−65.6(6)
5	C1−E−C51−C56	−37.6(1)	−35.0(3)	−30.0(5)
6	C1−E−C61−C62	−25.8(1)	−30.2(2)	−43.3(5)

[a] "E" represents Si, Ge, or Sn. Atom designations as in ORTEP diagram (Figure 2). [b] Data for SnPh from ref 23.

(30) Fair, C. K. *MolEN. An Interactive Intelligent System for Crystal Analysis*; Enraf-Nonius: Delft, The Netherlands, 1990.
(31) Craven, B. M.; Weber, H.-P.; He, X. M. *The POP Least-Squares Refinement Procedure*; University of Pittsburgh: Pittsburgh, PA, 1987.
(32) Becker, P. J.; Coppens, P. *Acta Crystallogr., Sect. A* **1974**, *30*, 129−147.
(33) Cromer, D. T.; Waber, J. T. *International Tables for X-ray Crystallography*; Kynoch Press: Birmingham, England, 1974; Vol. IV, pp 71−147 (present distributor, Reidel: Dordrecht, The Netherlands).
(34) Cromer, D. T.; Waber, J. T. *International Tables for X-ray Crystallography*; Kynoch Press: Birmingham, England, 1974; Vol. IV, pp 148−151 (present distributor, Reidel: Dordrecht, The Netherlands).
(35) Meier-Brocks, F.; Weiss, E. *J. Organomet. Chem.* **1993**, *453*, 33−45.

Table 3. Closest Contacts for SiPh, GePh, and SnPh in the Solid[a]

compd	no.	atom 1	atom 2	length, Å	length − VdW, Å
SiPh	1	C44	H25	2.816	−0.084
	2	C54	H14	2.795	−0.105
	3	H14	C54	2.795	−0.105
	4	H25	C44	2.816	−0.084
	5	C34	H44	2.859	−0.041
	6	H44	C34	2.859	−0.041
	7	C11	H55	2.898	−0.002
	8	H55	C11	2.898	−0.002
GePh	1	C54	H14	2.801	−0.099
	2	H14	C54	2.801	−0.099
	3	C62	H13	2.867	−0.033
	4	H13	C62	2.867	−0.033
	5	C34	H44	2.815	−0.085
	6	H44	C34	2.815	−0.085
SnPh[b]	1	C55	H14	2.981	−0.009
	2	H14	C55	2.891	−0.009
	3	C11	H55	2.838	−0.062
	4	C16	H55	2.878	−0.022
	5	H55	C11	2.838	−0.062
	6	H55	C16	2.878	−0.022
	7	C33	C33	3.388	−0.012

[a] Closest contacts shown are for one molecule in the unit cell (each unit cell contains two molecules, each with the same set of closest contacts). All close contacts are between atom 1 in one molecule and atom 2 in a molecule of an adjacent unit cell. [b] Data for SnPh from ref 23.

have the most favorable overlap with the electronic structure of the core ring. The geometric arrangement of the phenyl substituents gives the molecules propeller-like shapes and greatly influences the way in which the molecules can pack in the solid and, presumably, in the aggregates discussed below. The closest contacts of the 1,1-diphenyl-substituted metalloles are summarized in Table 3; the implications of the packing arrangements in terms of AIE of PL are discussed below.

B. UV−Vis Absorption and Emission Characteristics in Room-Temperature Fluid Solutions. In dilute fluid solution at room temperature, all six compounds have a large absorbance at about 250 nm and a distinct absorption band centered near 350 nm. The 350 nm band is attributed to $\pi-\pi^*$ transitions involving the π structure of the metallacyclopentadiene ring. A ring-opened derivative of SnMe does not show a 350 nm band.[23] The wavelengths of maximum absorbance show little dependence on the identity of the heteroatom or the nature of the solvent. The 1,1-diphenyl versions of the compounds show slight red-shifted absorbance maxima (5−7 nm) compared to their 1,1-dimethyl analogues. This observation is consistent with the findings of Tamao and co-workers,[11] who suggest that the 1,1-substituents on similar siloles affect both the LUMO and HOMO energy levels to a comparable extent, predominantly through an inductive effect rather than by perturbation through the $\sigma^*-\pi^*$ conjugation. A significant lowering of the LUMO energy for the 1,1-diphenylsiloles without a concurrent lowering of the HOMO was ascribed to the extended $\sigma^*-\pi^*$ conjugation over the phenyl rings on the silicon atom. In general, more electronegative 1,1-substituents tend to give longer absorption wavelengths, primarily by lowering the energy of the LUMO.[10,11] All six compounds are efficient absorbers. For each compound, the molar absorptivity at the 350 nm band varies little with the identity of the solvent. Average molar absorptivities (L mol^{-1} cm^{-1}) are 9800 for SiMe, 12 100 for GeMe, 10 200 for SnMe, 8800 for SiPh, 10 300 for GePh, and 9800 for SnPh (the quoted values represent averages over the solvents studied). The insensitivity of the absorption characteristics of the compounds to changes in solvent polarity, donor number, and acceptor number indicates that differences in polarity and/or electron density between ground and excited electronic states of the compounds are not large. Absorption wavelength maxima in fluid solutions at room temperature are included in Table 5 as averages across all of the solvents studied.

Table 4. Luminescence Quantum Yields (Φ_F) of the Metalloles at 0.01 mM in Various Solvents at Room Temperature

	tetrahydrofuran	dioxane	ethanol	benzene	methylene chloride	acetonitrile
SiMe	0.0010	0.0016	0.0009	0.0017	0.0008	0.0005
GeMe	0.0014	0.0028	0.0013	0.0031	0.0015	0.0008
SnMe	0.0003	0.0008	0.0002	0.0007	not measured	0.0000
SiPh	0.0018	0.0042	insoluble	0.0020	0.0014	0.0009
GePh	0.0029	0.0063	insoluble	0.0055	0.0026	0.0016
SnPh	0.0011	0.0014	insoluble	0.0012	0.0009	0.0004

All six compounds are weak emitters in dilute fluid solution, with luminescence quantum yields ranging from zero (SnMe in acetonitrile) to 0.0063 (GePh in dioxane). The wavelengths of maximum excitation closely match the absorption maxima. Luminescence yields are affected by solvent, heteroatom, and heteroatom substituents to greater extents than are the molar absorptivities. In solution, the quantum yields of the 1,1-diphenyl compounds are larger than those of their 1,1-dimethyl analogues. Of the solvents studied, the greatest quantum yields are observed in dioxane and benzene; the weakest luminescence is observed in acetonitrile. In fluid solution at room temperature, the germoles have the greatest PL quantum yields; the stannoles are by far the weakest emitters, with SnMe displaying negligible luminescence. Presumably, the heavy-atom effect of tin is primarily responsible for the poor-emission yields of the stannoles. It also has been observed that SnMe is the least-stable of the compounds in solution. Acetonitrile solutions of SnMe are particularly subject to degradation; experimental evidence indicates this most likely occurs via an acid-catalyzed ring opening reaction. Computational treatment of 2,5-dithienylmetalloles by Tamao and co-workers[7] indicates comparable HOMO and LUMO levels in the siloles, germoles, and stannoles. The three compounds studied had similar LUMO shapes, with lobes on the group 14 elements, suggesting that $\sigma^*-\pi^*$ conjugation plays an important role in all three, although the $\sigma^*-\pi^*$ conjugation occurs less effectively as the group 14 element becomes heavier, especially in the case of tin. This observation is attributed to less-efficient orbital interaction between the carbon π^* and the σ^* of the group 14 element as the latter gets larger and thus the carbon−heteroatom distance increases (carbon−heteroatom distances in the hexaphenylmetalloles, determined from the X-ray crystal structures, are found in Table 2).

Like the absorption wavelengths, emission wavelengths show little dependence on solvent. The 1,1-diphenyl compounds have emission maxima that are red-shifted compared

Table 5. Absorption (Abs) and Emission (Em) Wavelength Maxima and Luminescence Quantum Yields (Φ_F) of the Metalloles in Fluid Solution, Fluid Solution Aggregates (dioxane/water system), and SOA Glasses, at Room Temperature[a]

	fluid solution averages			fluid solution aggregate			SOA glass		
compd	Abs λ, nm	Em λ, nm	Φ_F	Abs λ, nm	Em λ, nm	Φ_F	Abs λ, nm	Em λ, nm	Φ_F
SiMe	357	484	0.0011	365	488	0.16	352	470	0.43
GeMe	353	470	0.0018	360	474	0.042	355	467	0.084
SnMe	353	486	0.0004	361	491	0.004	361	462	0.012
SiPh	364	505	0.0021	368	506	0.38	363	482	0.59
GePh	358	489	0.0038	362	487	0.10	357	467	0.20
SnPh	360	495	0.0010	366	505	0.010	363	483	0.038

[a] The fluid solution values are averages across the various solvents (refer to Table 4 for quantum yields in specific solvents). Metallole concentrations in all cases are approximately 0.01 mM.

Table 6. Stokes Shifts for the Metalloles in Various Media at Room Temperature[a]

compd	fluid solution (mean), nm	aggregate (dioxane), nm	SOA glass, nm	pure solid, nm
SiMe	127	123	118	103
GeMe	117	114	112	90
SnMe	132	130	101	NA
SiPh	141	138	119	122
GePh	130	125	110	97
SnPh	135	139	120	98

[a] Fluid solution values are averages across all solvents. All concentrations are 0.01 mM except pure solid. SnMe was not measured in pure solid.

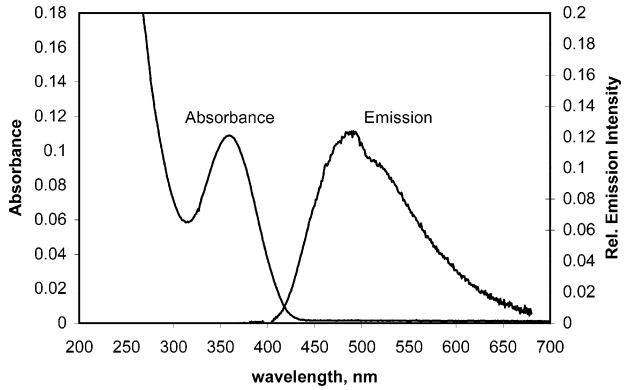

Figure 3. Absorption and corrected emission spectra of GePh in dioxane solution at room temperature. The apparent shoulder in the emission spectrum is an instrument artifact.

to the dimethyl analogues; the Si compounds show the greatest red shift between the dimethyl and diphenyl versions (21 nm), the Ge compounds are similar (19 nm), and the Sn compounds show the least red shift (9 nm). Relative PL quantum yields in various solvents are reported in Table 4; absorption and emission wavelength maxima and quantum yields averaged over all of the solvents studied are presented in Table 5. Stokes shifts for the compounds range from 117 to 135 nm (Table 6); shifts are slightly greater for the 1,1-diphenyl compounds than for their dimethyl analogues. Molar absorptivities and quantum yields are in good agreement with those reported previously for SiMe and SiPh.[10,36] All six compounds have similarly shaped absorption and emission bands; representative absorption and emission spectra (GePh) are shown in Figure 3.

C. Aggregation-Induced Enhancement (AIE) of Emission at Room Temperature. When the metalloles were

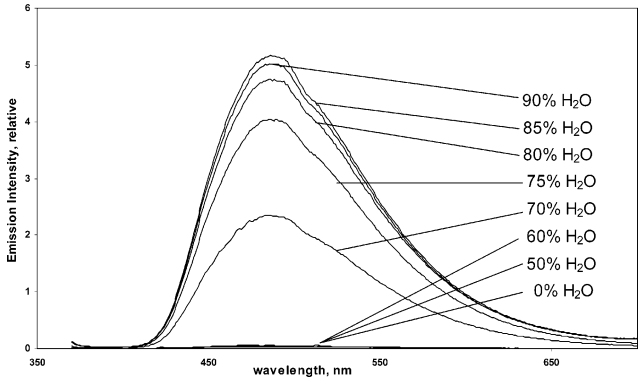

Figure 4. Emission spectra of SiMe aggregates in dioxane/water systems. Total SiMe concentration in each case was 0.01 mM.

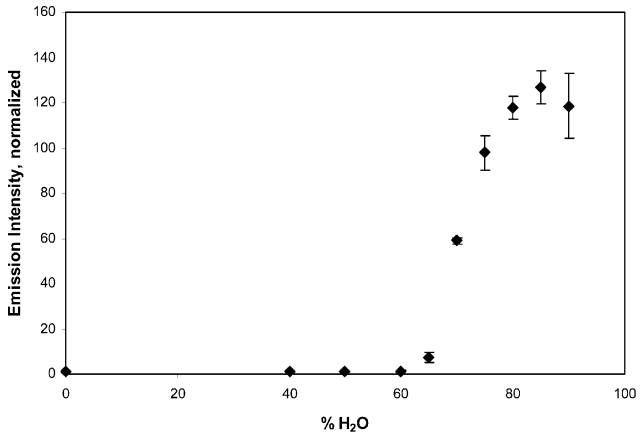

Figure 5. Emission intensity (normalized to nonaggregated 0% H_2O case = 1) as a function of % H_2O for SiMe in dioxane/water system. Error bars represent ± 1 standard deviation.

forced to aggregate in room-temperature mixed-solvent systems, a dramatic enhancement of luminescence emission was observed. The degree of enhancement was proportional to the amount of poor solvent (water) added to the system (and, therefore, to the degree of aggregation). The behavior of SiMe aggregates in a dioxane/water system, illustrated in Figures 4 and 5, is representative and stands in stark contrast to the typical behavior of aggregated fluorophores. Most luminescent compounds undergo aggregation-induced self-quenching due to the formation of excimers and other nonemissive species.[15,37] The behavior of anthracene, illustrated in Figure 6, is typical of most luminescent compounds. The enhancement effect was evident in metallole

(36) Hennig, H.; Heckner, K.-H.; Pavlov, A. A.; Kuzmin, M. G. *Ber. Bunsen-Ges. Phys. Chem.* **1980**, *84*, 1122−1124.

(37) Deans, R.; Kim, J.; Machacek, M. R.; Swager, T. M. *J. Am. Chem. Soc.* **2000**, *122*, 8565−8566.

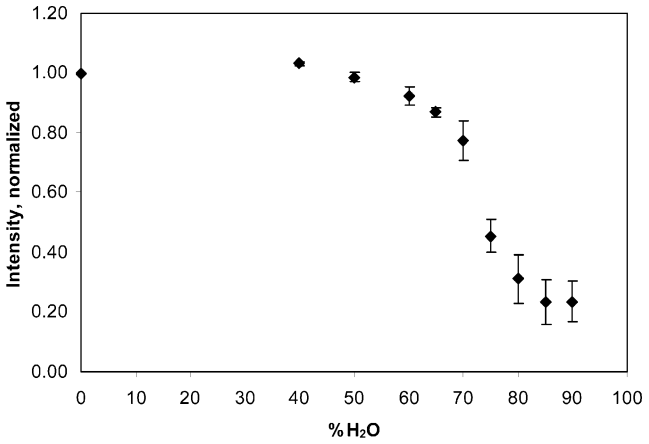

Figure 6. Emission intensity (normalized to 0% H_2O case = 1) of anthracene in ethanol/water mixtures. Error bars represent ±1 standard deviation.

systems with ≥60% water and reached a maximum at 85−90% (v/v) water. Although the germoles were the best emitters when molecularly dissolved in dilute fluid solution, the siloles showed the greatest aggregation-induced emission enhancement and were by far the strongest emitters when aggregated (this behavior is consistent with that observed by Tang and co-workers for similar siloles and germoles[16]). The luminescence quantum yields of the aggregates were as much as 300 times greater than those observed in dilute fluid solution, with no significant changes in the wavelengths of maximum emission. The greatest AIE effects were observed in dioxane/water systems. Only slightly less dramatic were the aggregation-induced emission enhancements observed in THF/water, ethanol/water, and acetonitrile/water systems. The ethanol/water systems were not explored in detail due to the limited solubility of SiPh, GePh, and SnPh in ethanol, and the acetonitrile/water systems received limited attention due to the apparent lack of stability of the aggregates in these mixtures. Table 5 contains a summary of the absorption maxima, emission maxima, and PL quantum yields of the aggregates in dioxane/water systems. The values in this table represent the 85% water case, the solvent composition that most often resulted in the greatest AIE effects.

D. Emission Behavior in Room-Temperature Glasses. When the metalloles were dispersed in rigid room-temperature SOA glasses at concentrations of approximately 0.01 mM, emission yields were greatly enhanced compared to similarly dilute fluid solutions and were approximately 1.5−3.7 times greater than those in the corresponding fluid solution aggregates. These experiments were completed in an attempt to distinguish the effects of restricted rotation (of the substituent phenyl rings) from possible aggregation-induced packing effects (with subsequent enhanced intermolecular interactions) as the primary cause of the increased emission from the aggregates. Rotational effects certainly are restricted in the rigid glass, but it is not clear whether the metalloles are aggregated to some extent. Although the glasses did not demonstrate the Tyndall effect scattering typical of the fluid solution aggregates, it is possible some degree of aggregation occurred, resulting from unfavorable interactions between the nonpolar metalloles and the polar SOA. These observations, and the possibility of nanoaggregate formation in the glasses, are consistent with those reported for PMMA thin films of 1-methyl-1,2,3,4,5-pentaphenylsilole[13] and silole-containing polyacetylenes,[19,20] indicating the same type of AIE mechanism is likely to be at work in both the SOA glasses and PMMA films. Luminescence characteristics, including quantum yields, for the compounds in SOA glasses are compiled in Table 5.

E. Emission Characteristics in Dilute Solutions at Low Temperatures. In a further attempt to isolate the effects of restricted rotation from intermolecular interactions, luminescence was observed from dilute dioxane solutions at approximately −20 and −196 °C. Because of the opacity of the frozen solutions, emission was observed using a front-surface accessory in the spectrofluorometer, and emission intensities were compared to those of the same solutions and SOA glasses observed under the same instrumental conditions at room temperature. Quantum yields were not determined. Emission intensities were significantly greater for the frozen solutions than for the corresponding room-temperature solutions and SOA glasses and inversely related to temperature. Relative emission intensities are collected in Table 7. Compared to the corresponding room-temperature fluid solutions, emission intensities increased by factors of 5−88 (depending on the metallole) at −20 °C and by factors of 32−134 at −196 °C. SnMe was not measured under these conditions. These observations are consistent with those reported by Tang and co-workers for linear poly(phenylenesilolene)s at low temperatures.[19,20]

F. Solid-Phase Emission Characteristics. Excitation maxima of pure pellets of the metalloles were red-shifted an average of 11 nm compared to dilute room-temperature fluid solutions, and emission maxima were blue-shifted an average of 17 nm, resulting in the smallest Stokes shifts of all the media (average 102 nm; Tables 6 and 8). These changes are attributed to changes in the population distribution of the vibrational states in the solids. Strong emission was observed from all compounds tested in the solid phase. Quantum yields were not calculated for the solids.

G. Estimated Excited-State Lifetimes in Room-Temperature Fluid Solution. Application of eq 1 to the metalloles in dilute room-temperature dioxane solutions resulted in the estimated excited-state lifetimes collected in Table 9. As the table shows, the lifetimes are estimated to be only tens of picoseconds. These compare reasonably well to the measured values of 79 ps for GeMe[28] and 150 ps for SiPh[21] but are somewhat shorter than the 400 ps values for SiMe and SiPh reported by Hennig et al.[36]

Discussion

The impressive increase in PL quantum yields of the metalloles in the fluid-phase aggregates is unusual, so it is of interest to determine the reasons these compounds defy the typical self-quenching behavior observed with the model compound, anthracene. Does the increase in emission yield of the aggregated metalloles result from intermolecular phenomena facilitated by the proximity of the molecules or from intramolecular phenomena? Intramolecular phenomena

Table 7. Relative Emission Intensity Comparison: Metalloles (0.01 mM) in Room Temperature and Frozen Dioxane Solutions, and Room-Temperature SOA Glasses[a]

	room temp solution		SOA glass		frozen solution (−20 °C)		frozen solution (−196 °C)	
compd	λ_{EM}, nm	intensity	λ_{EM}, nm	intensity	λ_{EM}, nm	intensity	λ_{EM}, nm	intensity
SiMe	481	0.105	471	0.920	469	2.282	467	3.347
GeMe	472	0.041	466	0.264	461	0.343	453	2.968
SnMe	490	0.004	486	0.067	469	0.028	451	0.464
SiPh	482	0.030	481	1.572	481	2.635	473	4.018
GePh	505	0.027	468	0.649	460	0.533	457	1.005
SnPh	513	0.014	482	0.053	469	0.0716	463	0.742

[a] For a given metallole, all measurements were made under the same conditions; thus, relative intensities for a given metallole can be compared directly.

Table 8. Excitation and Emission Maxima for Solid Pellets of the Metalloles[a]

compd	excitation maximum, nm	emission maximum, nm
SiMe	371	474
GeMe	370	460
SiPh	370	492
GePh	369	466
SnPh	369	467

[a] Pellets of SnMe were not prepared.

Table 9. Estimated Excited-State Lifetimes of the Metalloles in Room-Temperature Fluid Solution

compd	estimated lifetime, ps
SiMe	13
GeMe	28
SnMe	12
SiPh	65
GePh	68
SnPh	18

may include increased conjugation resulting from coplanarization of the substituent phenyl rings with the central cyclopentadiene ring[37] or restricted rotation/vibration phenomena. The similar enhancement of quantum yields in the aggregates and the SOA glasses suggests simple methods of exploiting this unusual behavior for the fabrication of optical devices but does not elucidate the mechanism responsible for the enhanced emission, since it cannot be guaranteed that the nonpolar metalloles are not aggregating to some extent in the polar SOA. The frozen dilute solution studies do tend to confirm that the enhancement of PL is achievable merely by restricting the rotational, vibrational, and collisional degrees of freedom of the metalloles. Other factors may be operative in the aggregates and SOA glasses, but certainly, the restricted rotational, vibrational, and collisional deactivation plays a major role.

For all of the metalloles, the absorption, excitation, and emission maxima for each compound are essentially the same in dilute fluid solution at room temperature and in fluid solution aggregates. In SOA glasses, there are small hypsochromic shifts in the emission wavelengths compared to those observed in dilute room-temperature fluid solutions, with no appreciable change in the excitation wavelengths. As a result, the Stokes shifts of the compounds change from averages of 130 nm in fluid solution to 128 nm in the aggregates and to 113 nm in SOA. The excitation maxima of the pellets are shifted to lower energy versus fluid solution values by an average of 7 nm, while the emissions are blue-shifted by an average of 17 nm, resulting in an average Stokes shift of 102 nm for the pellets. The wavelengths of maximum emission of the low-temperature dioxane solutions are blue-shifted to the greatest extent of all phases (an average of 28 nm vs room-temperature solutions). The degree of emission wavelength shift appears to be proportional to the rigidity of the medium, that is, the more rigid the medium, the higher the energy of emission. This effect is consistent with a reduction in the number of populated vibrational and/or rotational modes in the ground state.

The closest approaches of metallole molecules in the solid state, as determined by the crystal structures, are approximately 2.8 Å for the hexaphenylmetalloles (Table 3). There are eight closest contacts (less than the sum of the atoms' van der Waals' radii) between SiPh molecules in the solid, six between GePh molecules, and seven between SnPh molecules. In each case, there are two metallole molecules in the unit cell, and all of the closest contacts are to molecules in adjacent unit cells; none are to the other molecule within the given unit cell. In addition, all closest contacts are C−H contacts. Are these close contacts sufficient to perturb the photophysics of the emission of these species? The propeller-like shapes of the metalloles prevent them from approaching too closely to experience the kind of self-quenching observed in flat molecules such as anthracene, and steric effects would prevent significant coplanarization of the substituent phenyl rings. Indeed, the crystal structures demonstrate that significant PL-enhancing interactions among the phenyl groups, even in the solid, are unlikely. Thus, it is proposed that, even in fluid solution aggregates at room temperature, restricted molecular rotations are primarily responsible for the dramatic increase in PL quantum yields that are observed. Tang and co-workers have drawn similar conclusions for related siloles and germoles.[15,16,19−21]

In all media except dilute fluid solutions at room temperature, the PL quantum yields decrease in each series going from Si to Ge to Sn. This observation is attributed to increased spin−orbit coupling as the atomic number of the heteroatom increases. We propose that the intrinsic PL quantum yields follow this trend. In fluid solution, however, the Ge compounds have the greatest quantum yields. The fluid solution data can be rationalized if it is assumed that the siloles are more efficient at vibrational/rotational deactivation in fluid solution than the corresponding germoles.

Conclusions

The group 14 metalloles described here are weakly luminescent in dilute fluid solution at room temperature but

can be easily made to emit very strongly by changing the media in which they are dispersed. In particular, considerable enhancement of emission can be achieved by inducing aggregation of the metalloles in mixed solvent systems at room temperature. This considerable aggregation-induced enhancement of emission is contrary to the behavior of most luminescent compounds, which generally experience self-quenching of emission when forced to aggregate. Enhanced emission also is observed when the metalloles are dispersed in rigid room-temperature SOA glasses or in low-temperature solid solutions. The metalloles are highly luminescent in the pure solid state. The dramatic enhancement of emission in the aggregated, cooled, and glass phases is attributed to the restricted vibrational and rotational deactivation pathways available in these media. On the basis of the crystal structures, it is unlikely that the molecules approach closely enough in the aggregates or glasses to exhibit intermolecular enhancement mechanisms (e.g., $\pi-\pi$ interactions); in fact, the propeller-like shape of the molecules likely prevents the molecules from approaching closely enough to self-quench. This conclusion is consistent with the enhanced emission observed in frozen dilute solutions. The ability of these compounds to exhibit such greatly enhanced emission in aggregated and glass phases makes them very well suited for the preparation of a range of useful luminescent devices.

Acknowledgment. The authors thank Renee Plourde for her work on the ethanol and benzene systems. The financial support of the University of New England and the University of Southern Maine (USM) Department of Chemistry and USM Faculty Senate Research Grant Program is gratefully acknowledged.

Supporting Information Available: Crystallographic information files (CIFs) for GePh and SiPh; experimental conditions and ORTEP diagram for SiPh structure determination. This material is available free of charge via the Internet at http://pubs.acs.org.

IC049034O